

Gotta Hear Them All: Sound Source Aware Vision to Audio Generation

Wei Guo¹, Heng Wang¹, Jianbo Ma², Weidong Cai¹

¹University of Sydney ²Dolby Laboratories

wguo0893@uni.sydney.edu.au heng.wang@sydney.edu.au jianbo.ma@dolby.com tom.cai@sydney.edu.au

Abstract

Vision-to-audio (V2A) synthesis has broad applications in multimedia. Recent advancements of V2A methods have made it possible to generate relevant audios from inputs of videos or still images. However, the immersiveness and expressiveness of the generation are limited. One possible problem is that existing methods solely rely on the global scene and overlook details of local sounding objects (*i.e.*, sound sources). To address this issue, we propose a Sound Source-Aware V2A (SSV2A) generator. SSV2A is able to locally perceive multimodal sound sources from a scene with visual detection and cross-modality translation. It then contrastively learns a Cross-Modal Sound Source (CMSS) Manifold to semantically disambiguate each source. Finally, we attentively mix their CMSS semantics into a rich audio representation, from which a pretrained audio generator outputs the sound. To model the CMSS manifold, we curate a novel single-sound-source visual-audio dataset VGGSS3 from VGGSound. We also design a Sound Source Matching Score to measure localized audio relevance. By addressing V2A generation at the sound-source level, SSV2A surpasses state-of-the-art methods in both generation fidelity and relevance as evidenced by extensive experiments. We further demonstrate SSV2A’s ability to achieve intuitive V2A control by compositing vision, text, and audio conditions. Our generation can be tried and heard at <https://ssv2a.github.io/SSV2A-demo>.

1. Introduction

As multimedia consumption surges, generating sound for silent videos or still images attracts high demands in various industries [71]. The synthesized audio can complement a virtual reality scene [28], create Foley for films and games [11], and enrich single-modality visual contents for people with visual impairment [73]. By learning from the widespread visual-audio pairs in video data, recent methods can generate visually relevant audio clips for this vision-to-audio (V2A) task. However, most existing methods [12, 24, 37, 45, 53, 60, 61, 65, 69] only model the

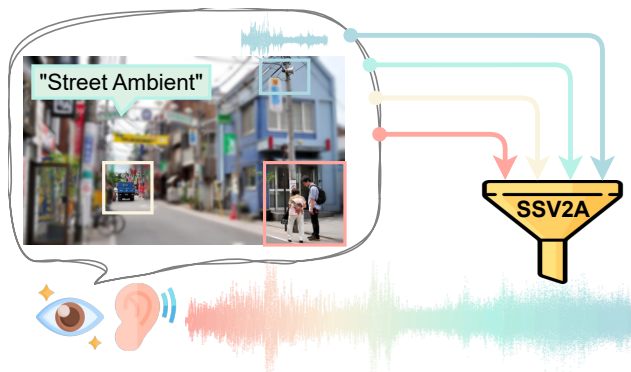


Figure 1. Our SSV2A perceives multimodal sound sources in a scene for V2A immersiveness and expressiveness.

mapping between the global visual scene and audio output while overlooking local details.

In reality, sound is produced and recognized from sounding objects, *i.e.*, **sound sources**, locally present in a soundscape [38]. For instance, in a street the sound comes from individual vehicles and passengers as illustrated in Fig. 1. Humans also perceive audio immersiveness and expressiveness from these sound sources in a visual scene [16]. In practice, audio engineers leverage individual sound sources to intuitively control sound synthesis [49].

Can a V2A synthesizer utilize **sound source-aware** conditions to obtain better generation quality and control? To answer this question, we present a **Sound Source-Aware V2A (SSV2A)** generator. We model our system in semantic spaces for learning efficiency and include multimodal conditions from text and audio to boost sound source controllability. As depicted in Fig. 1, the perception can also come from audio sound source as a loudspeaker and text source as “street ambient”. We present SSV2A’s pipeline in Fig. 2. SSV2A first **perceives** multimodal sound source conditions as CLIP [46] or CLAP [13] semantic embeddings with visual detection and cross-modal translation. We then project them to a Cross-Modal Sound Source (CMSS) Manifold to **disambiguate** each source semantic. By disambiguation, we require the CMSS manifold to (1) contrast the source

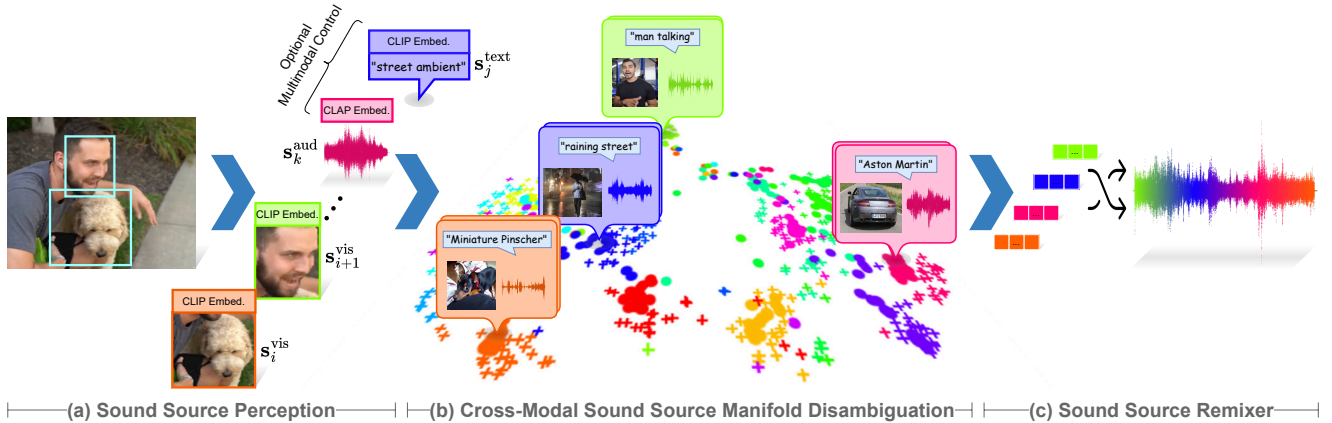


Figure 2. **Pipeline of SSV2A.** We perceive sound sources prompted by vision, text, or audio and disambiguate them in the semantically learned Cross-Modal Sound Source Manifold, after which we mix them to generate an audio clip with immersiveness and expressiveness.

semantics and (2) respect the audio characteristics of each sound source. After querying CMSS embeddings of individual sound sources, SSV2A learns an attention-based Sound Source Remixer to **mix** them into a CLAP audio embedding with rich sound source information. This representation is passed to a pretrained audio generator, AudioLDM [34], to synthesize the output audio waveform.

As the CMSS manifold contrastively learns from single-sound-source visual-audio pairs to disambiguate sound source semantics, we filter the VGGSound [3] data with visual detection to form a novel dataset, VGGSound Single Source (VGGSS3), that contains 106K high-quality single-sound-source visual-audio pairs. We also apply a novel Cross-Modal Contrastive Mask Regularization (CCMR) during manifold learning to retain rich CLIP-CLAP semantics by reducing CMSS contrastive influence on similar visual-audio sources with CLIP and CLAP priors. To effectively evaluate generation relevance, we introduce a Sound Source Matching Score (SSMS) to compute the F1 score of overlapping sound source labels on ground-truth and generated samples with an audio classifier.

Both objective and subjective results show that SSV2A outperforms state-of-the-art methods in V2A synthesis. We also demonstrate SSV2A’s intuitive generation control in experiments by flexibly compositing multimodal sound source prompts from vision, text, and audio.

In summary, our contributions are as follows:

- We present a novel V2A generation framework, SSV2A. To the best of our knowledge, this is the first work to address V2A synthesis at the sound-source level. Extensive experiments show that SSV2A achieves state-of-the-art results in both V2A generation fidelity and relevance.
- We explore how sound-source disambiguation can enhance SSV2A synthesis with the CMSS manifold, along with a novel CCMR mechanism to guide cross-modal

contrastive learning with foundation model priors.

- During manifold training, we curate a high-quality single-sound-source visual-audio dataset, VGGSS3, which supports learning of various sound-source-related tasks.
- In evaluating audio generation relevance, we introduce an effective SSMS metric aware of localized sound sources.
- We showcase multimodal sound source composition, a fresh audio synthesis paradigm that offers intuitive generation control over a wide range of usage scenarios.

2. Related Works

2.1. Vision-to-Audio Generation

Early V2A methods [5–7, 20, 44, 73] train a source-specific V2A model on each audio class and cannot generalize to open-domain V2A synthesis. As a precursor, recent SpecVQGAN [24] learns a discrete neural codec [14, 58] of source-agnostic audio features and autoregressively generates audio codes with a Transformer [59]. Following SpecVQGAN, Im2Wav [53] further details its audio codec into low-level and high-level features. MaskVAT [45] leverages a pretrained codec DAC [29] and predicts audio tokens with a Masked Generative Transformer [2]. Another line of methods employ Diffusion [23] models. CLIPSonic-IQ [12] queries CLIP [46] to condition its Diffusion process. Diff-Foley [37] contrastively learns a temporally-aligned visual-audio prior to guide video-audio synchronization. Draw-an-Audio [66] leverages loudness signal, text caption, and masked video conditions simultaneously. More recently, some methods bridge visual conditions to the prior of a pretrained audio generator for efficient V2A learning. V2A-Mapper [60] maps CLIP embeddings to CLAP [13] space, from which a pretrained AudioLDM [34] model synthesizes the audio signal. V2A-SceneDetector [67] extends V2A-Mapper to multi-scene video with a detection module. Seeing and Hearing [65] aligns ImageBind [17] vi-

sual embeddings to AudioLDM. FoleyCrafter [69] devises a timestamp predictor to enhance synchronization during bridging. Very recently, FRIEREN [61] and MMAudio [9] explore V2A generation with Rectified Flow Matching [36]. Most existing methods condition on global visual scenes for V2A synthesis. Some recent works [32] [31] leverage pixel-level conditions for V2A synthesis, partially describing visual sounding objects. In reality, human perceive object-level sound sources across modalities and time [38]. Such a sound source-aware V2A generator remains uninvestigated.

2.2. Contrastive Cross-Modal Alignment

Contrastive representation learning [18] has significantly advanced cross-modal representation alignment. CLIP [46] aligns text and image modalities by learning from abundant text-image pairs. Many aforementioned V2A methods [12, 45, 53, 60, 69] benefit from its semantically rich visual representations. Similarly, CLAP [13] learns from text-audio pairs and is used extensively in V2A generation [34, 35, 37, 60, 65, 66]. Aside from modality alignment, Diff-Foley [37] shows that it is possible to respect temporal alignment in the contrastive visual-audio representation to benefit video-audio synchronization. However, the entanglement of temporal features in this representation limits Diff-Foley in generalizing to image-to-audio synthesis. In this work, we focus on taming a contrastive representation for sound source disambiguation and leave the temporal alignment to a downstream temporal aggregation module.

3. Method

Approximating an audio distribution $Q(\mathbf{A}|\mathbf{a})$, the audio generator AudioLDM [34] generates audio signals \mathbf{A} from CLAP [13] audio semantics \mathbf{a} . For learning efficiency, we employ a pretrained Q and synthesize \mathbf{a} instead of \mathbf{A} . Conditioned on multimodal sound sources, our objective is to learn a conditional distribution:

$$P(\mathbf{a} | \{\mathbf{s}_i^{\text{vis}}\}, \{\mathbf{s}_j^{\text{text}}\}, \{\mathbf{s}_k^{\text{aud}}\}), \quad (1)$$

where $\{\mathbf{s}_i^{\text{vis}}\}$, $\{\mathbf{s}_j^{\text{text}}\}$, and $\{\mathbf{s}_k^{\text{aud}}\}$ denote respectively the semantic embedding sets of I visual sound sources, J text sources and K audio sources encoded with CLIP [46] or CLAP. We term the acquisition of these semantics as Sound Source Perception in Fig. 2 (a) and discuss it in Sec. 3.1.

The most straightforward way to approximate Eq. (1) is to train a standalone model that maps the perceived CLIP-CLAP semantics directly to \mathbf{a} . However, two CLIP features **ambiguate** this direct learning: (1) the CLIP image space models global visual context rather than contrasting individual objects, and (2) CLIP learns only from text-image data, which lacks awareness of the sources’ audio traits. As an efficient solution, we learn a Cross-Modal Sound Source (CMSS) manifold as illustrated in Fig. 2 (b) to project the

CLIP-CLAP embeddings to a joint semantic space where the local sound sources are **disambiguated**. We elaborate on this core stage of SSV2A in Sec. 3.2.

Finally, we attentively mix the CMSS embeddings together in Fig. 2 (c) to generate \mathbf{a} . This stage involves a Sound Source Remixer which we explain in Sec. 3.3.

3.1. Sound Source Perception

Recall Eq. (1). To extract $\{\mathbf{s}_i^{\text{vis}}\}$ from a global visual cue when no manual sound-source annotation is available, we pass each image through a visual detector and crop out the detected regions with predicted bounding boxes. These image regions are then embedded by CLIP. To obtain $\{\mathbf{s}_j^{\text{text}}\}$, we translate the CLIP text embeddings of text prompts to CLIP image space with a pretrained DALL·E-2 Prior [47] model to mitigate the visual-text domain gap [33] and ease downstream disambiguation. For $\{\mathbf{s}_k^{\text{aud}}\}$, we pass the audio prompts through CLAP to get embeddings.

3.2. Cross-Modal Sound Source Manifold

We contrastively learn the CMSS manifold from single-sound-source visual-audio pairs to project the perceived sound source semantics in Sec. 3.1 to a joint semantic space for disambiguation, as shown in Fig. 3 (a). The CMSS manifold naturally accommodates the multimodality of our perceptions due to the bridging of CLIP and CLAP.

Manifold Learning. We formulate two CMSS manifold projections $v(\cdot)$ and $\phi(\cdot)$ as:

$$\mathbf{e}_{\text{CLIP}} = v(\mathbf{v}), \mathbf{e}_{\text{CLAP}} = \phi(\mathbf{a}), \quad (2)$$

given a single-source visual-audio pair as (\mathbf{V}, \mathbf{A}) and its CLIP-CLAP embeddings as (\mathbf{v}, \mathbf{a}) . \mathbf{e} denotes the CMSS embedding. The projectors optimize a contrastive loss to attract visual-audio embeddings from the same sound-source pair and repel those from different sources. Following the symmetric contrastive guidance of CLAP [13], our main objective can be formulated for a batch of N pairs as:

$$\mathcal{L}_c = \frac{\ell_{\text{CLIP}}(\mathbf{C}) + \ell_{\text{CLAP}}(\mathbf{C})}{2}, \quad (3)$$

where $\ell_{\text{CLIP}}(\mathbf{C}) = \frac{1}{N} \sum_{i=0}^N \log \text{diag}(\text{softmax}(\mathbf{C}))$ penalizes off-diagonal similarities in similarity entries $\mathbf{C}_{ij} = \tau * [\mathbf{e}_{\text{CLIP}}^i \cdot (\mathbf{e}_{\text{CLAP}}^j)^\top]$. ℓ_{CLAP} follows ℓ_{CLIP} but swaps \mathbf{e}_{CLIP} and \mathbf{e}_{CLAP} in \mathbf{C}_{ij} . τ is a learned temperature parameter.

We define an auxiliary reconstruction $\chi(\cdot)$ to map the CMSS embeddings back to CLAP space, assisting their alignment with audio semantics. The reconstruction objective is designated for each visual-audio pair as:

$$\mathcal{L}_r = \frac{\|1 - \text{sim}(\mathbf{a}, \chi(\mathbf{e}_{\text{CLAP}}))\| + \|1 - \text{sim}(\mathbf{a}, \chi(\mathbf{e}_{\text{CLIP}}))\|}{2}, \quad (4)$$

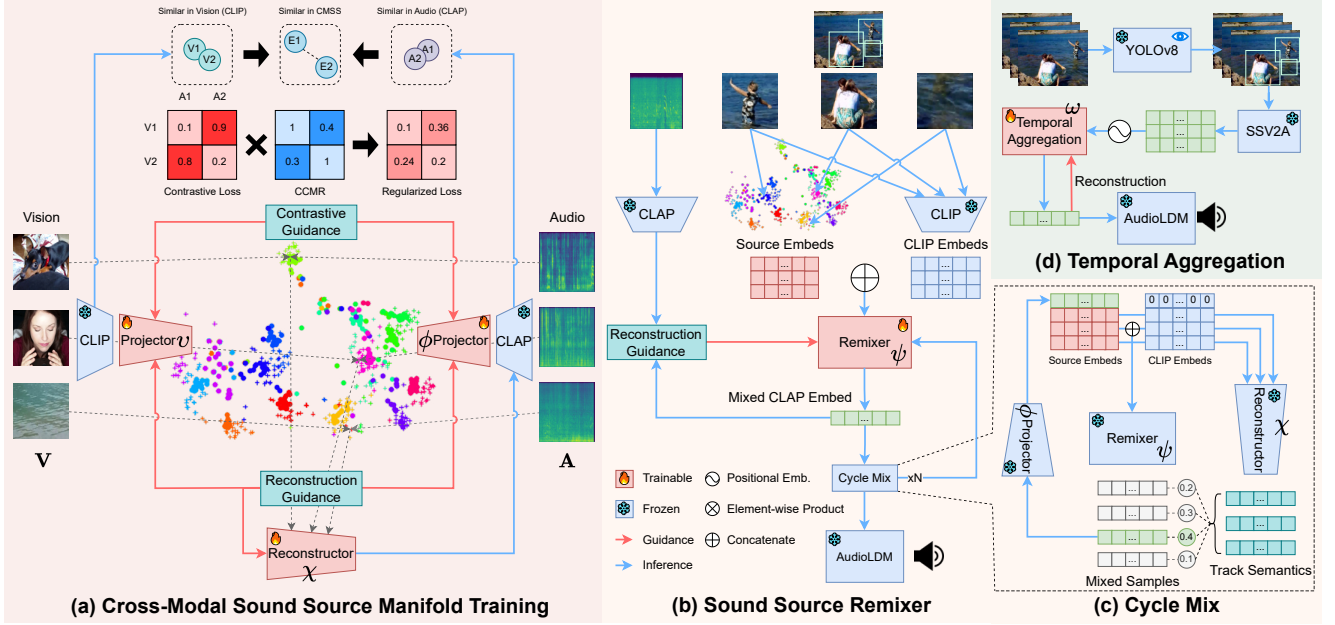


Figure 3. **Detailed Schematics of SSV2A Modules.** (a) We learn two projectors to map the CLIP-CLAP embeddings of single-source visual-audio pairs to a joint semantic space with contrastive guidance, forming our CMSS manifold. An auxiliary CLAP reconstruction encodes audio semantics into this manifold. (b) The Sound Source Remixer attends to the CMSS embeddings concatenated with their CLIP semantics, generating a single CLAP audio representation which is passed to AudioLDM. (c) We reuse the CMSS reconstructor to generate source-wise “track semantics” in CLAP space and refine the Remixer samples iteratively. (d) We train an additional Temporal Aggregation (TA) module to attend to positionally embedded SSV2A generations across video frames and enhance visual-audio synchronization.

where $\text{sim}(\cdot, \cdot)$ computes the cosine similarity.

We model $v(\cdot)$, $\phi(\cdot)$, and $\chi(\cdot)$ variationally with the reparameterization trick and add a Kullback-Leibler (K-L) divergence regularization term to each against the standard normal distribution as \mathcal{L}_{kl} . The final objective is then:

$$\mathcal{L}_{\text{fold}} = \mathcal{L}_c + \mathcal{L}_r + \lambda_1 \mathcal{L}_{kl}, \quad (5)$$

where λ_1 is a weight hyperparameter and \mathcal{L}_{kl} is the summed K-L losses. During training, we model all three modules $v(\cdot)$, $\phi(\cdot)$, and $\chi(\cdot)$ with residually connected MLPs and alternatively optimize the projectors and generator on each batch with $\mathcal{L}_{\text{fold}}$.

Cross-Modal Contrastive Mask Regularization. To avoid the loss of rich semantics from CLIP and CLAP due to small training data, we employ a Cross-Modal Contrastive Mask Regularization (CCMR) mechanism to weaken the contrastive guidance \mathcal{L}_c defined in Eq. (3) for similar cross-pair audio-visual samples. For each batch, we compute a CLIP-CLIP similarity matrix \mathbf{M}_{CLIP} and a CLAP-CLAP similarity matrix \mathbf{M}_{CLAP} per entry as:

$$\mathbf{M}_{\text{CLIP}}^{ij} = \text{sim}(\mathbf{v}_i, \mathbf{v}_j), \quad \mathbf{M}_{\text{CLAP}}^{ij} = \text{sim}(\mathbf{a}_i, \mathbf{a}_j). \quad (6)$$

The CCMR mask \mathbf{M} is then computed per entry as:

$$\mathbf{M}_{ij} = e^{-\alpha * (\text{clamp}(\mathbf{M}_{\text{CLIP}}^{ij} * \mathbf{M}_{\text{CLAP}}^{ij}))^\alpha}, \quad (7)$$

where $\text{clamp}(\cdot)$ restricts the mask entry to be within $[0, 1]$. This is a stretched exponential decay that grows smaller when both $\mathbf{M}_{\text{CLIP}}^{ij}$ and $\mathbf{M}_{\text{CLAP}}^{ij}$ increase. The hyperparameter α controls the decay curvature and steepness. We apply \mathbf{M} to the original contrastive similarity matrix \mathbf{C} with an element-wise multiplication as $\mathbf{C}_{ij}^* = \mathbf{C}_{ij} * \mathbf{M}_{ij}$.

Data Curation and Training. We filter visual-audio pairs from VGGSound [3] with a visual detection pipeline and obtain 106K single-sound-source visual-audio pairs as a novel dataset VGGSound Single Source (VGGSS3). We term the VGGSS3 pairs *curated pairs*. Additionally, we translate the single-source text-audio pairs from LAION-630K [64] to visual-audio pairs with a pretrained DALL·E-2 Prior [47] model. We term these pairs *translated pairs*. A Mean-Teacher [57] paradigm trains the CMSS modules with these pairs. Please refer to Appendix A.2.1 for our data curation and training details.

3.3. Sound Source Remixer

We employ a Sound Source Remixer function $\psi(\cdot)$ to mix the embeddings $\{e_m\}$ queried from the CMSS manifold in Fig. 3 (b), generating a CLAP audio representation with rich

sound source semantics as \mathbf{a}_{mix} . To leverage all the semantic features helpful for this task, we concatenate each \mathbf{e} with its CLIP embedding \mathbf{v} . Specifically, given a set of M sound sources, we formulate f_{mix} as:

$$\psi(\mathbf{x}_1, \mathbf{x}_2, \dots, \mathbf{x}_M) = \mathbf{a}_{\text{mix}}, \quad (8)$$

where $\mathbf{x}_i = \text{concat}(\mathbf{e}_m, \mathbf{v}_m)$ is the concatenated token for the m -th source. We model $\psi(\cdot)$ variationally to make it generative. The optimization objective is designed as:

$$\mathcal{L}_{\text{mix}} = \|1 - \text{sim}(\mathbf{a}, \mathbf{a}_{\text{mix}})\| + \lambda_2 \mathcal{L}_{kl}, \quad (9)$$

where \mathcal{L}_{kl} is the KL divergence from standard normal distribution, and λ_2 is a weight hyperparameter.

We model $\psi(\cdot)$ with a stack of self-attention layers and learn it from visual-audio pairs in VGGSound. The visual sources are perceived from each video’s central frame following Sec. 3.1. Each token sequence $\{\mathbf{x}_m\}$ is zero padded to a fixed length of $M = 64$. To enhance generation diversity, a Classifier-free Guidance [22] is applied during training by randomly zeroing out tokens. We replace the classic attention with Efficient Attention [54] and detail this architecture in Appendix A.2.2. During inference, we set $\mathbf{v} = \mathbf{0}$ for sound source conditions from audio modality.

Cycle Mix. Recall in Sec. 3.2 that we can also obtain a CLAP embedding $\mathbf{a}_{\text{src}} = \chi(\mathbf{e})$ for each sound source through the manifold’s reconstructor module. \mathbf{a}_{src} can be regarded as a set of source-wise audio semantics generated by our method. As one of our objectives for \mathbf{a}_{mix} is to have high relevance to each sound source, $\{\mathbf{a}_{\text{src}}^m\}$ are recycled to iteratively guide the generation of \mathbf{a}_{mix} . This mechanism, termed Cycle Mix, is illustrated in Fig. 3 (c) and Algorithm 1.

Algorithm 1 Cycle Mix

Require: $\{\mathbf{e}_m\}, \{\mathbf{x}_m\}$ \triangleright CMSS embs. and Remixer tokens
Require: T \triangleright user specified iterations
Require: N \triangleright user specified Remixer sample size
 $\mathbf{a}_{\text{mix}}^{\text{best}} \leftarrow \text{null}$ \triangleright best Remixer generation
 $s \leftarrow 0$ \triangleright best generation score
 $i \leftarrow 0$
while $i < T$ **do**
 $\mathbf{a}_{\text{src}}^m \leftarrow \chi(\mathbf{e}_m) \quad \forall m \in [1, \dots, M]$
 $\mathbf{a}_{\text{mix}}^n \leftarrow \text{sample}[\psi(\mathbf{x}_1, \dots, \mathbf{x}_{M+1})] \quad \forall n \in [1, \dots, N]$
 $\mathbf{d}_n \leftarrow \frac{1}{M} \sum \text{sim}(\mathbf{a}_{\text{mix}}^n, \mathbf{a}_{\text{src}}^m) \quad \forall n \in [1, \dots, N]$
if $\max(\mathbf{d}) > s$ **then**
 $\mathbf{a}_{\text{mix}}^{\text{best}} \leftarrow \mathbf{a}_{\text{mix}}^{\arg \max(\mathbf{d})}$
 $s \leftarrow r$
 $\mathbf{x}_{M+1} \leftarrow \text{concat}[\phi(\mathbf{a}_{\text{mix}}^{\text{best}}), \mathbf{0}] \quad \triangleright$ conditions next iter.
end if
 $i \leftarrow i + 1$
end while
return $\mathbf{a}_{\text{mix}}^{\text{best}}$

Temporal Aggregation. So far, the Sound Source Remixer learns an image-to-audio task. Following V2A-Mapper [60], we adapt it to the video-to-audio task with a downstream Temporal Aggregation (TA) function $\omega(\cdot)$ depicted in Fig. 3 (d). Instead of averaging the frame-wise semantics, we learn a nonlinear $\omega(\cdot)$. We evenly extract 64 frames along time from one video and generate a CLAP embedding for each of them. Each embedding is then positionally embedded with its timestamp. $\omega(\cdot)$ learns to fuse these embeddings into a temporally-aligned CLAP audio representation \mathbf{a} with the following loss:

$$\mathcal{L}_{\text{ta}} = \|1 - \text{sim}(\mathbf{a}, \omega(\text{pos}(\mathbf{a}_{\text{gen}}^1, \dots, \mathbf{a}_{\text{gen}}^{64}), t))\|, \quad (10)$$

where \mathbf{a}_{gen} denotes the SSV2A generated CLAP embeddings and $\text{pos}(\cdot, t)$ is the positional embedding function. The architecture of TA is a stack of self-attention layers.

4. Experiments and Results

4.1. Experimental Setup

Datasets. We train our teacher CMMS manifold modules on the VGG Sound Source (VGG-SS) [4] dataset. The student modules learn from (1) VGG-SS and (2) curated and translated visual-audio pairs described in Sec. 3.2. Since VGG-SS does not have an official train-test split, we randomly sample 4.5K pairs from it for training and form a test set with the remaining 500 pairs. We train the Sound Source Remixer modules following the provided train-test split on VGGSound [3], which contains 19K pairs across 310 audio categories. As VGG-SS is derived solely from VGGSound’s test set, its training samples are also VGGSound’s test samples. Therefore, we only test on the VGG-SS test split for fairness, which contains 38 multi-source pairs and 455 single-source pairs. We also test on two out-of-distribution datasets MUSIC [70] and ImageHear [53] to show SSV2A’s generalization capability. MUSIC contains 140 multi-source pairs with duet musical instrument performance, and 1034 single-source pairs with solo instrument. ImageHear has 101 images from 30 visual classes. We generate 10-second audio samples for all tests.

Implementation Details. We adopt the pretrained ViT-L/14 [42] for CLIP and the pretrained weights of audioldm-s-v2-full [34] for CLAP and AudioLDM. An open-source DALL·E-2 Prior model [30] trained on the Aesthetics [39] dataset translates the text-audio pairs. The visual detector in Sec. 3.1 is a YOLOv8x [27] model trained on the OpenImagesV7 [43] dataset with a 0.25 confidence threshold. We train all SSV2A modules with an AdamW optimizer of 1e-4 learning rate until convergence and fix the classifier-free guidance’s dropout rate to be 0.2. Please refer to our architecture details in Appendix A.2.

	Method	VGG-SS				MUSIC				ImageHear
		V-FAD↓	C-FAD↓	CS↑	SSMS↑	V-FAD↓	C-FAD↓	CS↑	SSMS↑	CS↑
Single-Source Generation	GroundTruth	0	0.171	13.199	10	0	0	13.906	10	-
	Oracle	1.400	9.983	12.071	5.752	6.430	25.422	12.861	7.777	-
	S&H	16.015	90.656	5.901	1.903	49.045	156.898	4.126	1.421	3.417
	S&H-Text	7.118	37.899	9.761	3.685	25.081	77.218	10.259	5.635	7.401
	Diff-Foley-Image	14.220	51.433	8.281	2.642	36.420	91.631	7.387	4.151	6.992
	Diff-Foley	7.212	39.309	11.045	4.099	27.633	79.068	9.286	5.899	-
	Im2Wav	7.573	29.213	11.011	4.451	26.344	57.596	8.374	6.214	10.758
	V2A-Mapper	1.666	13.583	<u>11.842</u>	<u>4.488</u>	7.245	<u>27.657</u>	<u>12.901</u>	<u>6.288</u>	<u>12.689</u>
	SSV2A (Ours)	<u>2.815</u>	<u>15.150</u>	12.215	4.936	<u>8.075</u>	25.390	13.859	7.330	13.930
Multi-Source Generation	GroundTruth	0	0.793	12.344	10	0	0	13.009	10	-
	Oracle	4.356	31.569	11.840	6.447	1.492	34.295	11.658	6.300	-
	S&H	21.447	121.371	6.594	2.568	27.661	175.708	3.979	0.986	-
	S&H-Text	12.678	81.944	9.573	4.026	9.887	105.529	9.149	5.223	-
	Diff-Foley-Image	19.633	99.661	8.276	2.474	15.254	111.848	7.371	3.950	-
	Diff-Foley	13.373	75.829	12.209	4.789	12.423	105.299	8.561	4.843	-
	Im2Wav	12.915	64.648	11.309	<u>5.132</u>	12.055	81.321	6.426	<u>5.357</u>	-
	V2A-Mapper	<u>10.228</u>	<u>59.660</u>	11.331	4.684	<u>4.490</u>	<u>48.665</u>	<u>11.126</u>	4.907	-
	SSV2A (Ours)	6.810	46.933	<u>11.744</u>	5.973	3.387	31.115	12.951	6.000	-

Table 1. **Objective comparisons.** The first and second places are **bolded** and underlined, respectively. The ImageHear test is not source-annotated and only CS is available for lack of ground-truth pairing audio with each image.

Method	Generation Relevance		Generation Fidelity	
	MOS↑	Std.	MOS↑	Std.
Diff-Foley-Image	1.775	0.799	1.125	0.173
Im2Wav	2.595	0.736	2.273	0.757
S&H-Text	2.358	0.845	2.460	0.748
V2A-Mapper	3.063	1.024	2.693	1.210
SSV2A (Ours)	4.080	0.527	4.098	0.459

Table 2. **Subjective comparisons.** Our method has the highest Mean Opinion Score (MOS) in both generation fidelity and relevance.

Method	WMAO ↓	
	Top-1	Top-5
Diff-Foley	1.227	1.127
FoleyCrafter	1.247	1.167
V2A-Mapper	1.299	1.197
Ours w/o TA	1.292	1.205
Ours	1.243	1.172

Table 3. **Synchronization tests on AVSync.** Red, orange, and brown mark first, second, and third placements.

Objective Metrics. We measure generation quality objectively from two perspectives: fidelity and relevance. For generation fidelity, we adopt the Fréchet Audio Distance (FAD) [48] with an open-source implementation [56] to obtain two metrics, V-FAD and C-FAD, respectively from VGGish [48] and CLAP [13] models. FAD measures the closeness of ground-truth and generated audio feature distributions. A low FAD score reflects high generation fidelity. For generation relevance, we first adopt the CLIP-Score (CS) which maps an audio’s CLAP embedding to the CLIP image space with a pretrained Wav2CLIP [63] model to compare its similarity with the paired image. For multi-source image-audio pairs in VGG-SS, we compute the av-

eraged CS between each sound source image and the paired audio. We compute CS on global images in other tests. A high CS score represents high generation relevance.

Matching Score. We observe that the CS relevance comparison, by mapping audio features to image domain, causes loss of audio information. As a result, our method often outperforms Oracle AudioLDM generations in CS scoring from Tab. 1. We propose a novel metric, Sound Source Matching Score (SSMS), that adopts an audio classifier BEATs [8] to respectively predict N localized sound source labels for ground-truth and generated audios. We regard intersected labels from the predicted sets as true positives, the

CMSS	CLIP	Single-Source Generation				Multi-Source Generation			
		V-FAD↓	C-FAD↓	CS↑	SSMS↑	V-FAD↓	C-FAD↓	CS↑	SSMS↑
✗	✓	39.622	122.127	3.987	1.385	34.378	119.692	5.574	1.579
✓	✗	17.949	96.045	6.049	1.213	7.689	48.776	11.156	5.553
✓	✓	2.815	15.150	12.215	4.936	6.810	46.933	11.744	5.973

Table 4. **Ablation of Sound Source Remixer conditions.** We achieve the best performance with both CMSS and CLIP semantics.

α	Single-Source Generation				Multi-Source Generation			
	V-FAD↓	C-FAD↓	CS↑	SSMS↑	V-FAD↓	C-FAD↓	CS↑	SSMS↑
0	13.612	73.849	5.838	1.149	17.053	98.747	5.580	1.342
0.35	2.815	15.150	12.215	4.936	6.810	46.933	11.744	5.973
0.65	2.877	16.194	11.860	4.356	9.788	61.565	11.397	4.658
1	3.323	16.740	11.299	4.075	10.098	60.810	11.585	4.237

Table 5. **Ablation of CCMR.** We achieve the best performance with $\alpha = 0.35$. This optimal setting is used throughout other experiments.

difference of ground-truth against generation as false negatives and the difference of generation against ground-truth as false positives. SSMS is computed as the F1 score of these statistics. We set $N = 10$ throughout experiments and show in Tab. 1 that SSMS distinguishes generation relevance more clearly than CS.

Weighted Mean Absolute Offset. To prove the efficacy of our TA mechanism for video-audio synchronization, we employ SynchFormer [25] to predict the temporal Weighted Mean Absolute Offset (WMAO) in seconds between the original video and the generated audio on the AVSync15 [68] dataset. We weight and sum the top-k predictions of SynchFormer with their confidence scores. A lower WMAO perceives smaller drifts between video-audio signals, indicating higher synchronization.

Subjective Metrics. Following recent works [45, 60, 69], we conduct a subjective listening test with 20 human evaluators. We randomly sample 40 central video frames from AudioSet Strong [21] and AVSBench [72], generating 10-second audio clips with each method. The test participants are asked to rate 20 of them for fidelity without visual cues. They then rate 20 samples for relevance given the visual conditions. We collect the ratings on a 5-point scale and compute the Mean Opinion Score (MOS) [51] to measure generation fidelity and relevance. Please see Appendix A.5 for the evaluation setup.

4.2. Baseline Evaluations

We compare our generator with four V2A methods: V2A-Mapper [60], Diff-Foley [37], Seeing and Hearing (S&H) [65] and Im2Wav [53]. Currently, V2A-Mapper holds state-

of-the-art generation fidelity and relevance. These methods require different visual conditions. For fairness, we modify some methods following Appendix A.1 but still keep their original versions in Tab. 1. For WMAO tests, we compare our method with video-to-audio methods V2A-Mapper, Diff-Foley and FoleyCrafter [69].

Objective Results. As illustrated in Tab. 1, our method achieves superior performance in most objective metrics for both in-distribution and out-of-distribution tests. For single-source generation, our SSV2A outperforms baselines in generation relevance and stays in top 2 for generation fidelity. For multi-source generation, SSV2A is superior in all metrics. Surprisingly, SSV2A achieves a higher CS in generation relevance than the Oracle baseline, which is assumed to have optimal performance for V2A methods involving AudioLDM. This effect is no longer observed in SSMS, demonstrating our new metric’s superiority in comparing audio generation relevance. Even though Diff-Foley and S&H-Text are unfair comparisons, SSV2A still surpasses them in both fidelity and relevance.

On the other hand, our method generates competitive video-audio synchronization as shown by the WMAO tests in Tab. 3. The ablation in TA mechanism shows that it is key to SSV2A’s temporal alignment capability. Moreover, the results indicate that our nonlinear TA function performs better than V2A-Mapper’s linear setup.

Subjective Results. In Tab. 2, we obtain the subjective results as Mean Opinion Score (MOS) from human evaluations. Our method outperforms baselines significantly in both generation fidelity and relevance. Since the random samples are images, we test on the Diff-Foley-Image instead of Diff-Foley because the latter only accepts video inputs. Moreover, we choose to test S&H-Text instead of

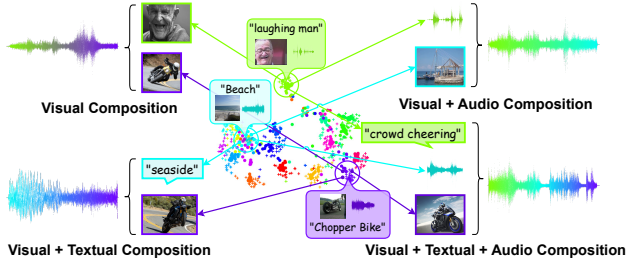


Figure 4. **Multimodal Sound Source Composition scenarios.** Our method can flexibly composite sound sources across visual, text, and audio modalities to guide V2A generation.

S&H to obtain the best generation performance Seeing and Hearing can achieve, even though it sees extra text captions.

4.3. Ablation Study

We conduct several ablation experiments to consolidate our claims in Sec. 3. We also provide an analysis on the learned CMSS manifold space and more ablations in Appendices A.3 and A.4.

Effect of CMSS Manifold. At the beginning of Sec. 3, we mention that SSV2A could learn to perform the V2A task without CMSS disambiguation. In order to prove the benefits of this disambiguation, we perturb the same Sound Source Remixer model with three different generation conditions: without CLIP embeddings, without CMSS embeddings, and with both embeddings. We train them on the same VGGSound data and evaluate the results with VGG-SS tests in Tab. 4. A significant performance drop is observed in both generation fidelity and relevance when the CMSS conditioning is suppressed. This ablation confirms that CMSS disambiguation benefits our V2A task.

Effect of CCMR. Recall that in Eq. (7) we have defined a hyperparameter α to control CCMR’s behavior. When $\alpha = 0$, the mask becomes an identity matrix and CCMR is stifled. We train the same CMSS manifold modules under four settings of α and conduct VGG-SS tests. Tab. 5 shows that with CCMR, we can enrich the CMSS semantics to benefit downstream generation. However, setting α to higher values degrades generation quality.

4.4. Multimodal Sound Source Composition

Since SSV2A accepts sound source prompts as vision, text, and audio, we can intuitively control its generation by (1) editing specific sound sources and (2) compositing sources across modalities. We term this novel generation control scheme Multimodal Sound Source Composition. We show-case four visually-related composition scenarios in Fig. 4. The composition results are best experienced via our website at <https://ssv2a.github.io/SSV2A-demo>.

Visual Composition. SSV2A can generate realistic audio

by composing visual sound sources. The result respects the supplied sources to render a convincing audio scene. For instance, we can synthesize a “motorbike riders laughing” audio from pictures of a motorbike and a laughing man.

Visual-Text Composition. SSV2A can further control the V2A generation with textual semantics. For example, we can supply a “motorbike” image and obtain a seaside riding audio with the text prompt “seaside”.

Visual-Audio Composition. We can achieve a similar style control with audio semantics. For example, we can accompany a “boat pier” image with a “talking” audio to synthesize audio of a busy pier.

Visual-Text-Audio Composition. Putting it altogether, we can synthesize audio with all three modalities involved. To test this feature, we have successfully produced a “coastline motorcycle racing” audio with a motorcycle image, a “crowd cheering” text, and a “beach” audio.

Comparison with Cascaded Composition. One could cascade video-to-audio and text-to-audio models to generate source-specific audio clips and overlay them together. We show that our SSV2A composition offers crucial interaction, context and style awareness when integrating sound sources, which are unachievable with this cascaded approach. Please see Appendix A.6 for details.

5. Limitations and Conclusion

In this work, we explore the feasibility of learning a sound source-aware V2A generator, SSV2A, that supports multimodal conditioning. By explicitly modeling the source disambiguation process with a contrastive cross-modal manifold on single-source visual-audio pairs, we are able to significantly boost our method’s generation fidelity and relevance. Consequently, SSV2A achieves state-of-the-art V2A performance in both objective and subjective evaluations. Moreover, we demonstrate the intuitive control of our generator in various composition experiments of sound source conditions from vision, text, and audio. To accompany the learning of our sound source disambiguation, we curate a new single-sound-source visual-audio dataset VGGSS3. Additionally, we contribute a novel Sound Source Matching Score that measures audio generation relevance more clearly than the existing CLIP-Score. Two limitations exist in SSV2A. First, we address the video-to-audio synchronization in SSV2A with a naive temporal module. Existing works [25, 26] show that temporal alignment is a nontrivial problem due to the sparsity of synchronization cues in both time and space. Second, we observe that SSV2A is less sensitive to audio conditioning than visual or text inputs. We suspect that this phenomenon is due to the lack of CLIP semantics when the Sound Source Remixer is prompted with audio conditions. Please see Appendix A.7 for our proposed solutions for these limitations.

Appendix

A.1. Baseline Modifications

We feed the entire video to Diff-Foley [37] for audio generation, which is an unfair comparison for other methods. This baseline is named Diff-Foley in our tables. Alternatively, we pad each central frame of these videos to 10 seconds and feed them to Diff-Foley, which results in a fairer baseline named Diff-Foley-Image. Note that Diff-Foley has also seen significantly more training data than VGGSound [3] offers, since it is also trained on Audioset-V2A [37], which offers 390K extra video-audio pairs.

We choose Seeing and Hearing [65] (S&H)’s image-to-audio (I2A) branch as a baseline. However, we notice this branch also depends on image text captioned from a large vision-language model, QWEN [1]. The text modality creates extra information in the I2A task, which is unfair for other methods since V2A-Mapper [60] and our SSV2A can also utilize the captions to refine results. Therefore, we rename the unfair version of S&H as S&H-Text, and suppress the QWEN captions to generate the fair set of baseline results, which is named S&H in experiments.

We directly generate results from Im2Wav [53] as it is focused on the image-to-audio task only. We also leave the setup of V2A-Mapper unchanged. Additionally, we obtain oracle generation results in the VGG-SS [4] and MUSIC [70] tests by passing the ground-truth audio clips through CLAP [13] and then AudioLDM [34]. We name this baseline Oracle. Aside from the ground-truth audio, the Oracle results can be regarded as generated from an audio synthesis model that exhausts AudioLDM’s potential for audio synthesis. We expect any method utilizing AudioLDM for downstream generation, *i.e.*, our SSV2A and V2A-Mapper, to be inferior in performance against Oracle.

A.2. Model Training and Architectures

A.2.1. Cross-Modal Sound Source Manifold

Architecture. We employ residually connected MLPs for the Cross-Modal Sound Source (CMSS) projectors and reconstructor, as shown in Fig. 5 (a). We choose the ELU function for activations and the dropout probability as 0.2. To implement the reparameterization trick, we append two respective linear layers at each module’s head to infer the estimated mean and variance. The output CMSS embeddings are sampled from a multivariate normal distribution with respect to these estimated parameters. The CMSS manifold’s semantic dimension is fixed to be 768. The CLIP-ViT-L/14 dimension is 768 and the CLAP dimension is 512. The neuron numbers for each module’s linear layers are reported in Tab. 6. We conduct ablation experiments in Appendix A.4.2 to obtain this optimal setup.

Module	Linear Layer Neurons
CLIP Projector	768×2, 1536×2, 3072×2
CLAP Projector	768×2, 1536×2, 3072×2
Reconstructor	768×2, 896×2, 1024×2, 2048×2

Table 6. **Neuron numbers for each CMSS module.** Note that we add a residual connection every two layers.

Data Curation. We filter source-unannotated visual-audio pairs from VGGSound [3] with an open-vocabulary object segmentor, CLIP as RNN (CaR) [55], keeping the pairs where only one visual region is segmented. The confidence threshold of CaR is set to 0.5. We use the VGGSound category labels as segmentation vocabulary. CaR’s pixel-level segmentations are abstracted into bounding boxes to capture fuller visual content. We crop each video’s central frame with the predicted bounding box to pair with its audio clip and verify the data quality by manually reviewing 10 results from each category. The resulted VGGSS3 dataset has 106514 samples across 221 sound source categories, which promises audio diversity. One potential bias is that the curated sound sources have unbalanced category frequencies with a max of 946 and a min of 100. We intend to release a balanced version of VGGSS3 alongside the current version.

Additionally, we regard the SFX text-audio pairs from FSD50K [15], Epidemic Sound Effects [41], and BBC Sound Effects [40] in the LAION-630K [64] dataset as single-source since they have succinct label-like text captions. We translate their CLIP text embeddings to CLIP image space with the DALL-E-2 Prior [47] model to pair with their CLAP audio embeddings.

Mean-Teacher Training. Recall Sec. 3.2. The only manually-annotated single-source visual-audio pairs for our learning purpose are from the VGG Sound Source (VGG-SS) [4] dataset. The curated and translated pairs we collect can be regarded as noisy. We follow a Mean-Teacher [57] paradigm to train the CMSS Manifold for extra robustness. A teacher model is overfitted on the VGG-SS pairs to supervise another student model which sees the augmented/pseudo pairs during training. The teacher weights are updated by an exponential mean average schedule from student weights at each batch. We further filter out curated/translated pairs regarded as extremely noisy from student training by computing the cosine similarity between each pair’s visual-audio CMSS embeddings with the teacher model and discarding the low-similarity ones adaptively with an elbow-finding algorithm Kneedle [50].

A.2.2. Sound Source Remixer

Efficient Attention. We adopt the Efficient Attention [54] architecture in place of classical attention in the

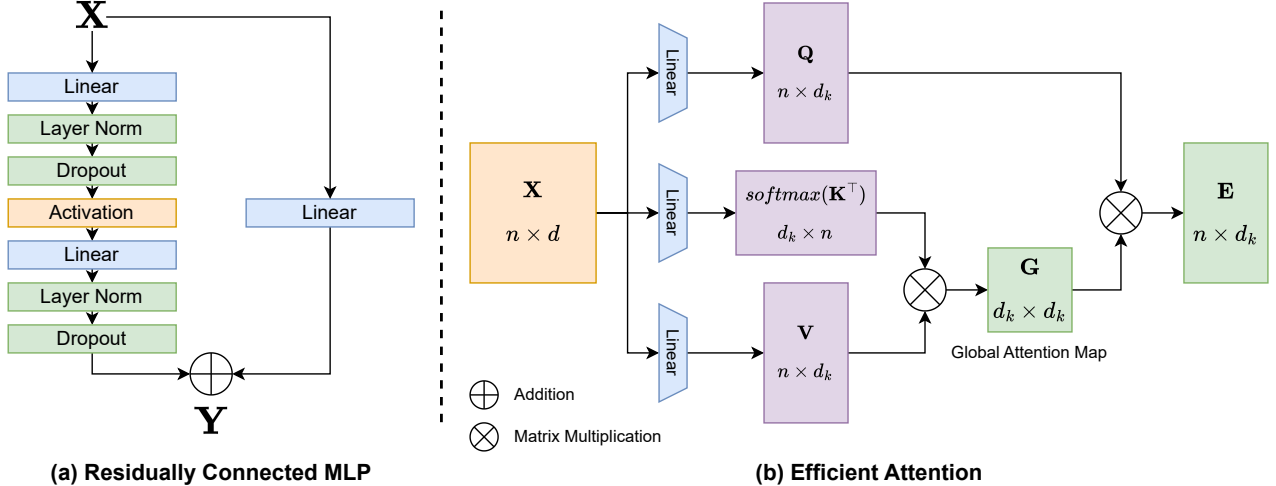


Figure 5. **Architecture of key module components.** We show a single instance instead of batch inference in (b).

Sound Source Remixer and Temporal Aggregation modules, which is shown in Fig. 5 (b). Instead of multiplying the query \mathbf{Q} and key \mathbf{K}^\top together for pairwise attention, the Efficient Attention computes a global attention map with value \mathbf{V} as $\text{softmax}(\mathbf{K}^\top)\mathbf{V}$. The global attention map emphasizes the global context of tokens, which is desired since we already have rich individual audio semantics and only intend to mix them globally.

Architecture. Recall Eq. (8). We assign a learned [cls] token at the head of each token sequence for the Sound Source Remixer’s prediction. The tokens first travel through a stack of attention modules, where each module contains an Efficient Attention layer followed by a feed forward network and an ELU activation. The [cls] token is then passed to two MLP heads to respectively estimate the mean and variance of the mixed CLAP audio embeddings. We then sample these embeddings from a normal distribution with these estimated parameters. The embeddings are further normalized with respect to their l_2 -norms to respect the original representation format of CLAP. Each MLP head is three-layer with [768, 640, 512] neurons and ELU activations. We use only one Efficient Attention layer following the optimal setup from ablation experiments in Appendix A.4.3.

Temporal Aggregation Architecture. The Temporal Aggregation (TA) module employs the same optimal architecture setup as the Sound Source Remixer. We use the following formula to compute the positional embeddings:

$$\text{pos}(2i, t) = \sin\left(\frac{t}{1024^{2i/512}}\right), \quad (11)$$

$$\text{pos}(2i + 1, t) = \cos\left(\frac{t}{1024^{2i/512}}\right), \quad (12)$$

where i denotes the embedding position and t is the integer timestamp of the video frame in $[1, 64]$. 1024 is fixed to be the positional embedding’s frequency resolution, and 512 is the output CLAP embedding’s dimension. To keep the model generative, we also model the TA module variationally with two prediction heads similar to those of the Sound Source Remixer.

A.3. Manifold Analysis

We conduct a manifold analysis to better understand the behaviors of CMSS manifold (abbreviated as manifold below). Ideally, we would like to observe the following traits from this manifold: (1) modality gap between audio and visual sound sources is closed, and (2) clustering forms naturally for similar audio-visual sound sources. The first trait confirms the cross-modal alignment of CMSS embeddings. The second trait manifests the manifold’s capability to disambiguate sound sources. To examine these effects, we randomly select 20 samples from each of the 16 top-occurring classes in the curated VGGs3 and report three experiments: visualizations, modality alignment tests, and clustering tests. We show that all three experiments support the existence of both traits in the manifold.

A.3.1. Visualizations

t-SNE Visualizations. Our visualizations are illustrated in Fig. 6. To visualize the unprocessed CLIP and CLAP embeddings of sampled visual-audio pairs, we reduce the CLIP

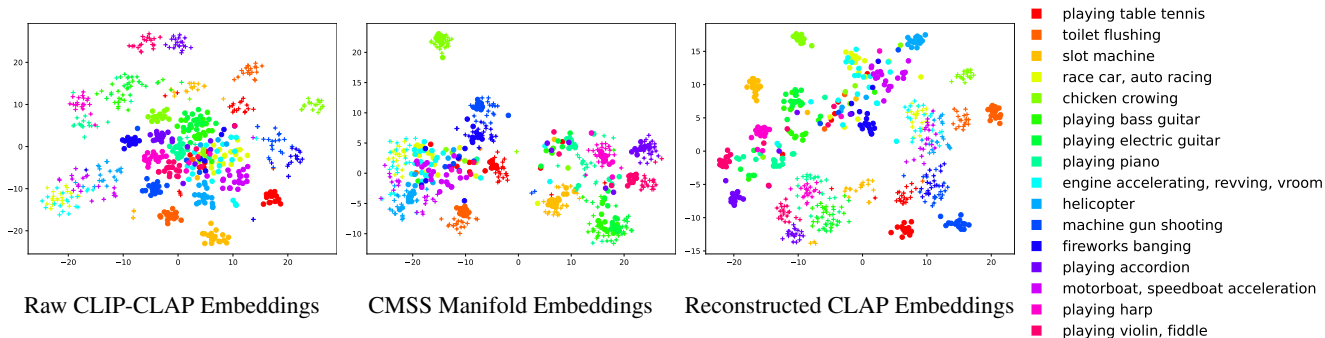


Figure 6. **t-SNE visualizations of visual-audio modality alignment.** The first figure visualizes raw CLIP-CLAP embeddings, the second depicts their remapped CMSS manifold embeddings and the third illustrates reconstructed CLAP embeddings from CMSS manifold. The circles mark visual embeddings while the crosses mark audio embeddings.

embeddings from 768 to 512 dims by Principal Component Analysis and visualize them together with the CLAP embeddings in t-SNE. We then respectively visualize the manifold embeddings of these samples and their reconstructed CLAP embeddings. It can be observed that modality gap is closed in CMSS manifold embeddings since the visual and audio embeddings are pulled towards each other. Furthermore, a natural clustering forms for each audio category in the manifold space.

Although both desired traits are still present in the reconstructed CLAP embeddings, we observe that the modality gap is larger and clustering is less prominent. Therefore, we choose to operate the Sound Source Remixer on manifold embeddings instead of the reconstructed CLAP embeddings for V2A synthesis.

Sound Source Similarity Visualization. We assign each visual sample to a cluster based on its audio class label. Average linkages in terms of cosine similarity are computed between clusters. We then filter these linkages with a > 0.4 threshold to visualize clusters that are very close to each other as a chord diagram in Fig. 7. We observe that our CMSS embeddings encode audio traits of sound sources as well as visual traits, which is the objective of our auxiliary reconstruction in Sec. 3.2. For instance, although a machine gun is visually different from fireworks, our manifold picks up the information that they share audio similarity. Likewise, the musical instruments are more similar in manifold space than other sound sources.

A.3.2. Modality Alignment Tests

Discriminant Test. We randomly select 4 audio categories and conduct a discriminant test on each in Tab. 7. These results are also visualized as a canonical plot in Fig. 8. The discriminant model is a wide linear binary classifier to predict whether a given sample is from the visual or audio modality. We observe that this classifier works per-

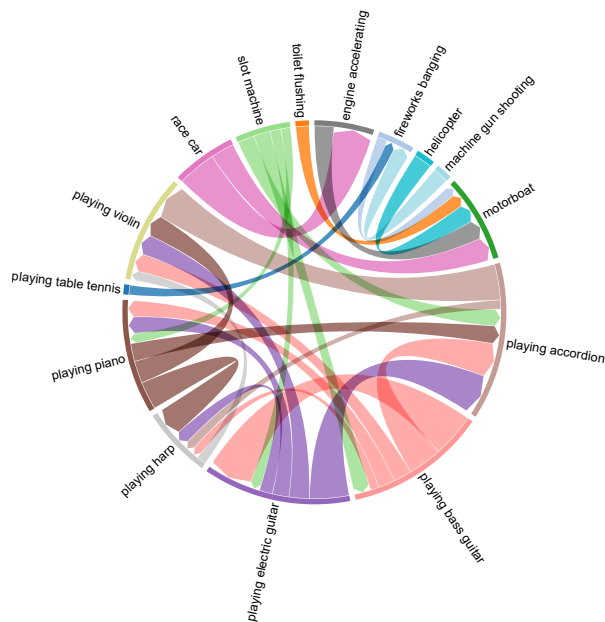


Figure 7. **Chord diagram of CMSS sound source similarities.** Wider chords indicate higher similarities between sources.

fectly on raw embedding samples but fails to classify the CMSS embeddings with a low Entropy R^2 (classification contingency) and high $-2 \log$ -likelihood (classification uncertainty). This discriminant test supports the manifold’s ability to close the modality gap between visual and audio data distributions, as the discriminant classifier is significantly confused after the manifold remapping of CLIP and CLAP embeddings.

A.3.3. Clustering Tests

Partition Coefficient Test. To examine whether our manifold embeddings have a stronger clustering tendency than the raw CLIP-CLAP embeddings, we evaluate Partition Co-

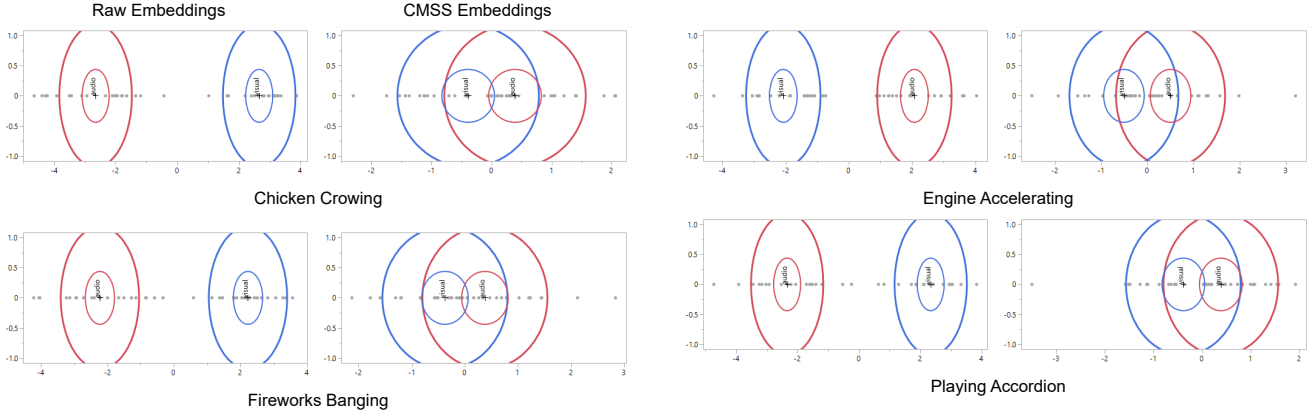


Figure 8. **Canonical plots of discriminant test.** The red inner circle marks the 95% confidence interval and the red outer circle marks the 50% normal contour of audio samples. The blue circles denote the visual samples.

Category	Embedding	Percent Misclassified \uparrow	Entropy $R^2 \downarrow$	-2 Log-Likelihood \uparrow
Chicken Crowing	Raw	0.000	0.996	0.201
	CMSS	35.000	0.106	49.587
Engine Accelerating	Raw	0.000	0.985	0.846
	CMSS	32.500	0.100	49.884
Fireworks Banging	Raw	0.000	0.999	0.048
	CMSS	35.000	0.146	47.369
Playing Accordion	Raw	0.000	0.984	0.889
	CMSS	35.000	0.107	49.530

Table 7. **Statistics of discriminant test.** There are 20 visual samples and 20 audio samples in each category.

Embeddings	Partition Coefficient \uparrow
Raw CLIP-CLAP	8.473
CMSS Manifold	12.615
Reconstructed CLAP	12.800

Table 8. **Partition Coefficient test.** The manifold’s reconstructed CLAP embeddings have the highest partition coefficient.

efficient (PC) [19] as a clustering validation index. Our PC is computed as:

$$PC = \frac{1}{N} \sum_{i=1}^N \sum_{j=1}^M u_{ij}^2, \quad (13)$$

where N is the sample size, M is the number of clusters and u_{ij} is the membership value of sample i to cluster j . Unlike the classic situation, where clusters are not assigned, we do have this information beforehand as the samples’ audio class labels. As such, we find the centroid of each cluster by taking the average of its samples, and define u as the cosine similarity between each sample and each centroid.

Moreover, since cosine similarity can have negative values whose squaring confuses PC, we linearly rescale the cosine similarity from $[-1, 1]$ to $[0, 1]$. We find that both manifold embeddings and the reconstructed CLAP embeddings obtain significantly higher PCs than the raw embeddings, as recorded in Tab. 8. This evaluation supports our claim that the manifold processing enhances clustering of sound source semantics.

A.4. More Ablations

A.4.1. Ablation of Cycle Mix

The Cycle Mix algorithm has two adjustable parameters: the number of iterations and the the sampling size of remixed CLAP embeddings in each iteration. We conduct 8 VGG-SS tests to observe the effect of Cycle Mix parameters. These ablations are illustrated in Tab. 9. When the iteration is 1 and sampling size is 1, we directly obtain the Remixer’s output without Cycle Mix. Higher sample size and iterations lead to better multi-source generations while single-source performance slightly drops. Setting the parameters too high compromises performance in both gener-

Sample Size	Iterations	Single-Source Generation				Multi-Source Generation			
		V-FAD↓	C-FAD↓	CS↑	MS↑	V-FAD↓	C-FAD↓	CS↑	MS↑
1	1	2.683	<u>14.869</u>	12.364	5.048	6.864	47.219	11.945	5.868
4	4	2.762	14.687	12.356	4.921	6.476	48.758	11.721	5.868
4	64	2.713	14.980	12.377	<u>5.042</u>	6.814	48.789	<u>11.912</u>	<u>5.921</u>
64	4	<u>2.710</u>	15.069	<u>12.390</u>	5.037	6.813	<u>46.963</u>	11.907	<u>5.921</u>
64	64	2.815	15.150	12.215	4.936	6.810	46.933	11.744	5.973
64	256	2.720	15.567	12.190	4.912	<u>6.755</u>	47.657	11.708	5.816
256	64	2.762	15.098	12.404	4.943	6.890	49.605	11.624	5.789
256	256	2.876	15.728	12.060	5.022	7.220	47.373	11.577	5.684

Table 9. **Ablation of Cycle Mix.** We choose both sample size and iterations to be 64 as the optimal parameter setup.

CMSS Variant	Projector Layers				Reconstructor Layers			
A	768×2, 1536×2				768×2, 896×2, 1024×2			
B	768×2, 1536×2, 3072×2				768×2, 896×2, 1024×2, 2048×2			
C	768×2, 1536×4, 3072×2				768×2, 896×3, 1024×3, 2048×2			
CMSS Variant	Single-Source Generation				Multi-Source Generation			
	V-FAD↓	C-FAD↓	CS↑	MS↑	V-FAD↓	C-FAD↓	CS↑	MS↑
A	6.684	42.423	7.974	3.220	9.036	54.437	10.699	4.868
B	2.815	15.150	12.215	4.936	6.810	46.933	11.744	5.973
C	6.945	26.035	9.868	3.993	11.343	59.819	9.908	4.763

Table 10. **Ablation of CMSS architectures.** We choose model variant B as the optimal parameter setup.

ation tasks. Since this work’s primary focus is multi-sound-source V2A synthesis, we determine a sample size of 64 and an iteration count of 64 as the optimal parameter setup and use it throughout other experiments.

A.4.2. Ablation of CMSS Architectures

We find the optimal architectures of the CMSS manifold modules through ablation experiments illustrated in Tab. 10. These ablations are performed by training the SSV2A pipeline with different CMSS module configurations and the same Sound Source Remixer. We observe that shallower projectors and reconstructor underfit on the training data while deeper modules tend to overfit. Consequently, we choose CMSS model variant B in Tab. 10 to be our optimal setup and use it throughout other experiments.

A.4.3. Ablation of Remixer Architecture

The optimal setup of the Sound Source Remixer’s architecture is found through ablations recorded in Tab. 11. Increasing the number of attention layers slightly increases single-source generation performance. However, the multi-source generation quality is significantly sacrificed as attention layers stack deeper. Since our work’s primary focus is to tackle the multi-sound-source V2A generation problem, we choose the one-attention-layer architecture as the opti-

mal setting for the Sound Source Remixer. We use the same architecture for the Temporal Aggregation module.

A.5. Setup of Subjective Evaluation

We disseminate an online survey for the subjective evaluation and collect results from 20 participants to measure generation fidelity and relevance of our method along with baselines. The baseline methods include Im2Wav, Diff-Foley-Image, S&H-Text, and V2A-Mapper as described in Appendix A.1. In the first survey section, we ask the participants to sign a consent form as illustrated in Fig. 12 (a). The non-consenting participants are screened out without any data collection. In the second section, we ask 20 fidelity-rating questions without visual cues following Fig. 12 (b). To unify the comparison context, we include a short tag in the question describing the ground-truth audio content. For each generated sample, the testee is asked to give out fidelity rating on a 1-5 scale. In the third section, we ask 20 relevance-rating questions given the visual condition used during generation, which is depicted in Fig. 12 (c). The ratings are also collected on a 1-5 scale.

After data collection, we thoroughly anonymize the participant information to deidentify any personal data. We then compute the Mean Opinion Score (MOS) [51] respec-

Attention Layers	Single-Source Generation				Multi-Source Generation			
	V-FAD↓	C-FAD↓	CS↑	MS↑	V-FAD↓	C-FAD↓	CS↑	MS↑
1	2.815	15.150	12.215	4.936	6.810	46.933	11.744	5.973
2	2.685	14.839	12.545	5.116	8.634	52.697	11.583	5.105
4	2.378	14.021	12.716	4.916	8.119	55.639	11.056	5.395

Table 11. **Ablation of the Sound Source Remixer architecture.** We choose one attention layer as the optimal setup.

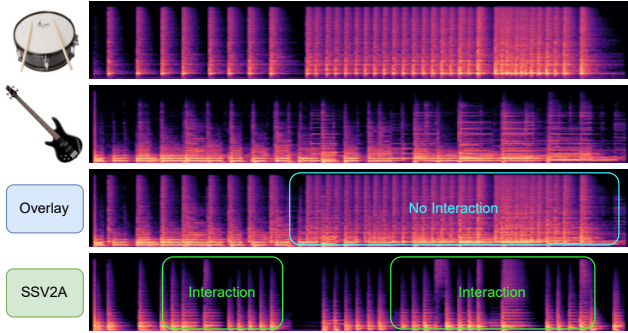


Figure 9. **Example of interaction awareness.** Our composition arranges drum and bass sounds into interactive music.

tively from the fidelity and relevance ratings.

A.6. Why Not Cascaded Composition?

The most straightforward way to composite multimodal sound sources into a single audio is to generate an audio track for each source condition via video-to-audio or text-to-audio models and overlay them together. However, such a cascading audio synthesis system lacks interaction, context and style awareness when integrating multiple sound sources, which are keys to a convincing audio scene. We show with qualitative examples in this section that our SSV2A composition achieves these features. These examples are best experienced on our website at the Composition Comparisons section.

A.6.1. Interaction Awareness

We generate a drum-only audio clip and a bass-only clip with SSV2A. Simply overlaying these clips yields a mixed track with no interactions between these instruments, which is shown in Fig. 9. With our SSV2A composition, we are able to generate an appealing piece of drum-bass music with rich interactions.

A.6.2. Context Awareness

We generate audio clips of a normal speech and an academic conference in Fig. 10. Cascaded composition synthesizes an audio clip with conflicting talkers and no conference room reverb. Our SSV2A composition properly transfers

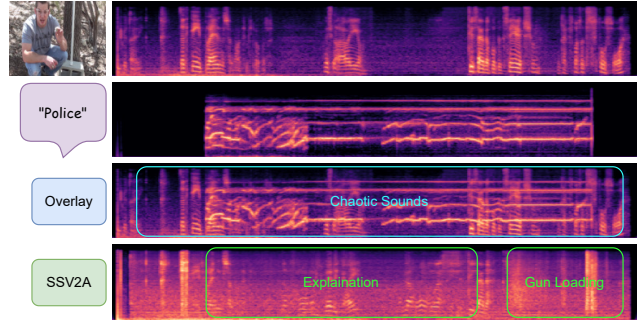


Figure 10. **Example of context awareness.** Our composition transforms a normal talking man into a police officer on duty.

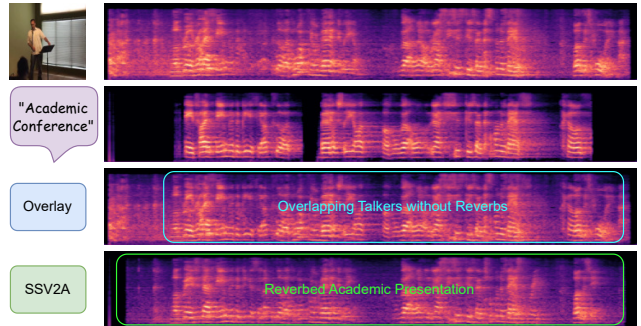


Figure 11. **Example of style awareness.** Our composition changes a normal speech into an academic presentation with conference room reverb.

the speech style into a reverberated academic presentation.

A.6.3. Style Awareness

In Fig. 11, we generate an audio clip of a talking man and another clip of police activities. The cascaded composition yields chaotic sounds as the police event context is not perceived. Our SSV2A composition successfully picks up this global cue and generates a police officer’s voice followed by a gun loading/shooting sound to indicate police events.

A.7. Future Improvements on Limitations

A.7.1. Temporal Synchronization

Our simple TA module has shown decent synchronization capability by attending to global audio scene semantics, as

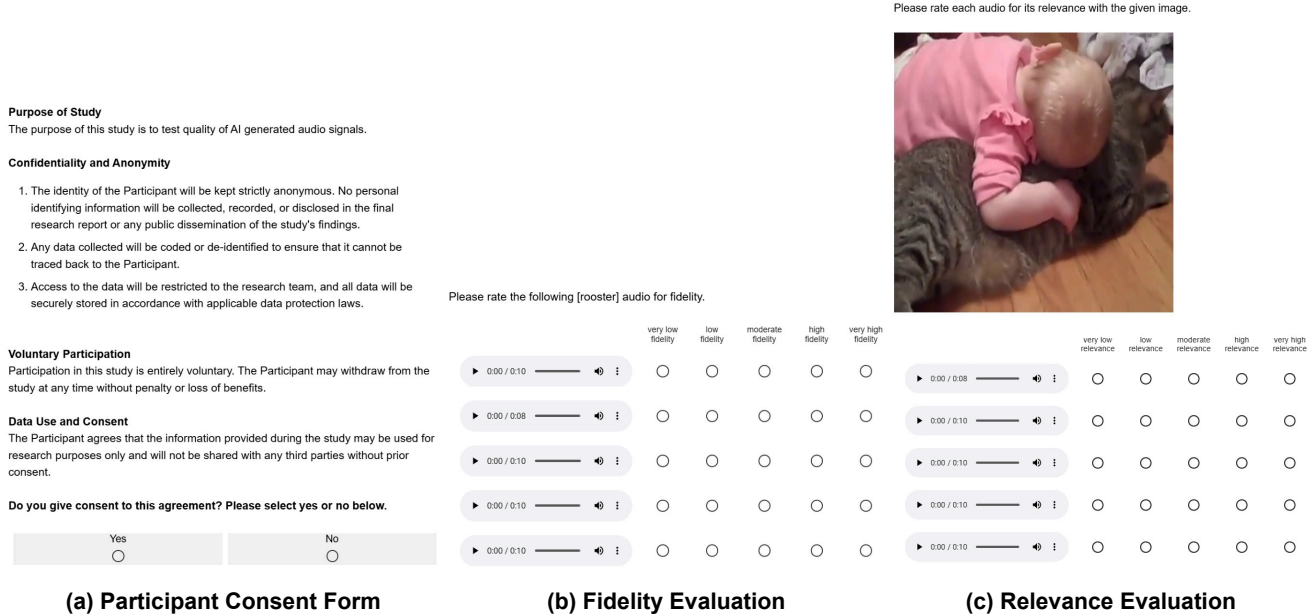


Figure 12. Screenshots of subjective survey. Each row of circles prompts a single-choice question to the testee.

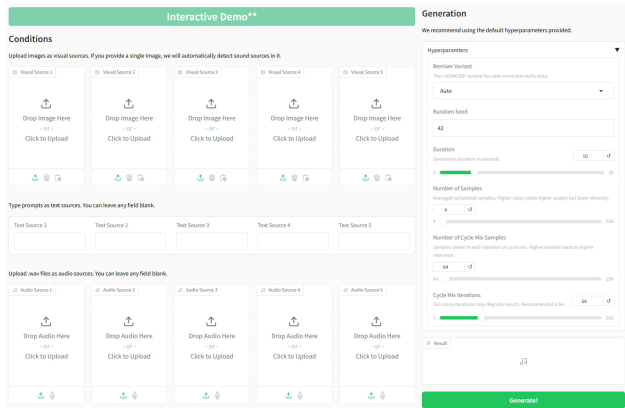


Figure 13. Screenshot of web demo application. Please visit our website and click the demo button to access this interface.

evidenced by WMAO evaluations in the Tab. 3. In reality, each sound source can have different temporal “activation” intervals in an audio scene. For example, a dog may bark in only the first three seconds of a video, followed by a baby laughing. In future works, we propose to perceive each sound source’s activations locally in time, similar to the tracklet detection [10] concept in video multi-object tracking. With this finer-grained temporal aggregation approach, we aim to further enhance SSV2A’s temporal alignment performance.

A.7.2. Sensitivity of Audio Conditioning

As stated in the limitations section, the lower sensitivity of our method’s audio conditioning compared to other modalities’ input is due to the lack of CLIP semantics for audio sound source inputs. An existing method, Wav2CLIP [63], translates CLAP audio embeddings to highly relevant CLIP embeddings. However, it operates on ViT-B/32 instead of ViT-L/14, which is the CLIP variant SSV2A employs. In future works, we plan to train a Wav2CLIP model compatible with SSV2A to address the audio sensitivity issue.

A.8. Implementation

We upload the implementation and pretrained weights of SSV2A to github at <https://github.com/wguo86/SSV2A>. Please follow the readme instructions to set up a virtual environment and execute the designated scripts.

A.9. Web Demo Instructions

We implement a web application for interactive demonstration, as illustrated in Fig. 13. The left panel supports entries of generation conditions from image, text and audio. The right panel offers further hyperparameter tuning. We host this application on our own machine via a secure internet tunnel, strictly avoiding any collection of user data.

A.10. Ethical Statement

Our human evaluation is strictly anonymized without collecting any sensitive personal data. We also obtain explicit

verbal consent from participants by asking them to sign a data collection agreement form before survey and screening out non-consenting participants. We intend to make our curated dataset, VGGs3, publicly available to contribute to the visual-audio research community. Our V2A method complements videos and images with convincing audio tracks. Its application may have malicious outcomes in deepfake [62] multimedia products if used without censorship. Multiple multimedia deepfake detection approaches have been proposed including audio deepfake detection [52]. We are committed to contribute ample generation samples for strengthening the learning of these detectors.

References

- [1] Jinze Bai, Shuai Bai, Yunfei Chu, Zeyu Cui, Kai Dang, Xiaodong Deng, Yang Fan, Wenbin Ge, Yu Han, Fei Huang, et al. Qwen technical report. *arXiv preprint arXiv:2309.16609*, 2023. 9
- [2] Huiwen Chang, Han Zhang, Lu Jiang, Ce Liu, and William T Freeman. MaskGIT: masked generative image transformer. In *CVPR*, pages 11315–11325, 2022. 2
- [3] Honglie Chen, Weidi Xie, Andrea Vedaldi, and Andrew Zisserman. VGGsSound: A large-scale audio-visual dataset. In *ICASSP*, pages 721–725, 2020. 2, 4, 5, 9
- [4] Honglie Chen, Weidi Xie, Triantafyllos Afouras, Arsha Nagrani, Andrea Vedaldi, and Andrew Zisserman. Localizing visual sounds the hard way. In *CVPR*, pages 16867–16876, 2021. 5, 9
- [5] Kan Chen, Chuanxi Zhang, Chen Fang, Zhaowen Wang, Trung Bui, and Ram Nevatia. Visually indicated sound generation by perceptually optimized classification. In *ECCV Workshop*, 2018. 2
- [6] Lele Chen, Sudhanshu Srivastava, Zhiyao Duan, and Chenliang Xu. Deep cross-modal audio-visual generation. In *Proceedings of the on Thematic Workshops of ACM Multimedia 2017*, pages 349–357, 2017.
- [7] Peihao Chen, Yang Zhang, Mingkui Tan, Hongdong Xiao, Deng Huang, and Chuang Gan. Generating visually aligned sound from videos. *IEEE Transactions on Image Processing*, 29:8292–8302, 2020. 2
- [8] Sanyuan Chen, Yu Wu, Chengyi Wang, Shujie Liu, Daniel Tompkins, Zhuo Chen, Wanxiang Che, Xiangzhan Yu, and Furu Wei. BEATs: audio pre-training with acoustic tokenizers. In *ICML*, pages 5178–5193, 2023. 6
- [9] Ho Kei Cheng, Masato Ishii, Akio Hayakawa, Takashi Shibuya, Alexander Schwing, and Yuki Mitsufuji. Taming multimodal joint training for high-quality video-to-audio synthesis. In *CVPR*, 2025. 3
- [10] Gioele Ciaparrone, Francisco Luque Sánchez, Siham Tabik, Luigi Troiano, Roberto Tagliaferri, and Francisco Herrera. Deep learning in video multi-object tracking: A survey. *Neurocomputing*, 381:61–88, 2020. 15
- [11] Balandino Di Donato and Iain McGregor. The digital Foley: what Foley artists say about using audio synthesis. In *Audio Engineering Society Conference: AES 2024 International Audio for Games Conference*. Audio Engineering Society, 2024. 1
- [12] Hao-Wen Dong, Xiaoyu Liu, Jordi Pons, Gautam Bhatnagary, Santiago Pascual, Joan Serrà, Taylor Berg-Kirkpatrick, and Julian McAuley. CLIPsonic: text-to-audio synthesis with unlabeled videos and pretrained language-visual models. In *IEEE Workshop on Applications of Signal Processing to Audio and Acoustics (WASPAA)*, pages 1–5, 2023. 1, 2, 3
- [13] Benjamin Elizalde, Soham Deshmukh, Mahmoud Al Ismail, and Huaming Wang. CLAP learning audio concepts from natural language supervision. In *ICASSP*, pages 1–5, 2023. 1, 2, 3, 6, 9
- [14] Patrick Esser, Robin Rombach, and Bjorn Ommer. Taming transformers for high-resolution image synthesis. In *CVPR*, pages 12873–12883, 2021. 2
- [15] Eduardo Fonseca, Xavier Favory, Jordi Pons, Frederic Font, and Xavier Serra. FSD50K: an open dataset of human-labeled sound events. *IEEE/ACM Transactions on Audio, Speech, and Language Processing*, 30:829–852, 2021. 9
- [16] William W Gaver. An ecological approach to auditory event perception. *Ecological Psychology*, 5(1):1–29, 1993. 1
- [17] Rohit Girdhar, Alaaeldin El-Nouby, Zhuang Liu, Mannat Singh, Kalyan Vasudev Alwala, Armand Joulin, and Ishan Misra. ImageBind: one embedding space to bind them all. In *CVPR*, pages 15180–15190, 2023. 2
- [18] Raia Hadsell, Sumit Chopra, and Yann LeCun. Dimensionality reduction by learning an invariant mapping. In *CVPR*, pages 1735–1742, 2006. 3
- [19] Maria Halkidi, Yannis Batistakis, and Michalis Vazirgiannis. On clustering validation techniques. *Journal of Intelligent Information Systems*, 17:107–145, 2001. 12
- [20] Wangli Hao, Zhaoxiang Zhang, and He Guan. CMCAN: a uniform framework for cross-modal visual-audio mutual generation. In *AAAI*, 2018. 2
- [21] Shawn Hershey, Daniel PW Ellis, Eduardo Fonseca, Aren Jansen, Caroline Liu, R Channing Moore, and Manoj Plakal. The benefit of temporally-strong labels in audio event classification. In *ICASSP*, pages 366–370, 2021. 7
- [22] Jonathan Ho and Tim Salimans. Classifier-free diffusion guidance. In *NeurIPS Workshop*, 2021. 5
- [23] Jonathan Ho, Ajay Jain, and Pieter Abbeel. Denoising diffusion probabilistic models. In *NeurIPS*, pages 6840–6851, 2020. 2
- [24] Vladimir Iashin and Esa Rahtu. Taming visually guided sound generation. In *BMVC*, 2021. 1, 2
- [25] Vladimir Iashin, Weidi Xie, Esa Rahtu, and Andrew Zisserman. Synchformer: efficient synchronization from sparse cues. In *ICASSP*, pages 5325–5329, 2024. 7, 8
- [26] Vladimir E. Iashin, Weidi Xie, Esa Rahtu, and Andrew Zisserman. Sparse in space and time: Audio-visual synchronization with trainable selectors. In *BMVC*, 2022. 8
- [27] Glenn Jocher, Ayush Chaurasia, and Jing Qiu. Ultralytics YOLOv8, 2023. Software. 5
- [28] Angelika C Kern and Wolfgang Ellermeier. Audio in vr: Effects of a soundscape and movement-triggered step sounds on presence. *Frontiers in Robotics and AI*, 7:20, 2020. 1

- [29] Rithesh Kumar, Prem Seetharaman, Alejandro Luebs, Ishaan Kumar, and Kundan Kumar. High-fidelity audio compression with improved RVQGAN. In *NeurIPS*, pages 27980–27993, 2023. 2
- [30] LAION. <https://huggingface.co/nousr/conditioned-prior/tree/main/vit-l-14/aesthetic>, 2024. Website. 5
- [31] Tingle Li, Baihe Huang, Xiaobin Zhuang, Dongya Jia, Jiawei Chen, Yuping Wang, Gopala Anumanchipalli, Zhuo Chen, and Yuxuan Wang. Object-aware audio-visual sound generation. *OpenReview*, 2024. 3
- [32] Zhaojian Li, Bin Zhao, and Yuan Yuan. Cyclic learning for binaural audio generation and localization. In *Proceedings of the IEEE/CVF Conference on Computer Vision and Pattern Recognition*, pages 26669–26678, 2024. 3
- [33] Weixin Liang, Yuhui Zhang, Yongchan Kwon, Serena Yeung, and James Zou. Mind the gap: understanding the modality gap in multi-modal contrastive representation learning. In *NeurIPS*, pages 17612–17625, 2022. 3
- [34] Haohe Liu, Zehua Chen, Yi Yuan, Xinhao Mei, Xubo Liu, Danilo Mandic, Wenwu Wang, and Mark D Plumbley. AudioLDM: Text-to-audio generation with latent diffusion models. In *ICML*, pages 21450–21474, 2023. 2, 3, 5, 9
- [35] Haohe Liu, Yi Yuan, Xubo Liu, Xinhao Mei, Qiuqiang Kong, Qiao Tian, Yuping Wang, Wenwu Wang, Yuxuan Wang, and Mark D Plumbley. AudioLDM 2: learning holistic audio generation with self-supervised pretraining. *IEEE/ACM Transactions on Audio, Speech, and Language Processing*, 32:2871–2883, 2024. 3
- [36] Kingchao Liu, Chengyue Gong, and Qiang Liu. Flow straight and fast: Learning to generate and transfer data with rectified flow. In *ICLR*, 2023. 3
- [37] Simian Luo, Chuanhao Yan, Chenxu Hu, and Hang Zhao. Diff-Foley: synchronized video-to-audio synthesis with latent diffusion models. In *NeurIPS*, pages 48855–48876, 2023. 1, 2, 3, 7, 9
- [38] Stephen McAdams. Recognition of sound sources and events. *Thinking in sound: The cognitive psychology of human audition*, pages 146–198, 1993. 1, 3
- [39] Naila Murray, Luca Marchesotti, and Florent Perronnin. AVA: a large-scale database for aesthetic visual analysis. In *CVPR*, pages 2408–2415, 2012. 5
- [40] Marianna Nezhurina. <https://huggingface.co/datasets/marianna13/BBCSoundEffects>, 2024. Website. 9
- [41] Marianna Nezhurina. https://huggingface.co/datasets/marianna13/epidemic_sound_effects, 2024. Website. 9
- [42] OpenAI. <https://github.com/openai/CLIP>, 2022. Website. 5
- [43] OpenImagesV7. <https://storage.googleapis.com/openimages/web/index.html>, 2024. Website. 5
- [44] Andrew Owens, Phillip Isola, Josh McDermott, Antonio Torralba, Edward H Adelson, and William T Freeman. Visually indicated sounds. In *CVPR*, pages 2405–2413, 2016. 2
- [45] Santiago Pascual, Chungshin Yeh, Ioannis Tsiamas, and Joan Serra. Masked generative video-to-audio transformers with enhanced synchronicity. *arXiv preprint arXiv:2407.10387*, 2024. 1, 2, 3, 7
- [46] Alec Radford, Jong Wook Kim, Chris Hallacy, Aditya Ramesh, Gabriel Goh, Sandhini Agarwal, Girish Sastry, Amanda Askell, Pamela Mishkin, Jack Clark, Gretchen Krueger, and Ilya Sutskever. Learning transferable visual models from natural language supervision. In *ICML*, pages 8748–8763, 2021. 1, 2, 3
- [47] Aditya Ramesh, Prafulla Dhariwal, Alex Nichol, Casey Chu, and Mark Chen. Hierarchical text-conditional image generation with CLIP latents. *arXiv preprint arXiv:2204.06125*, 2022. 3, 4, 9
- [48] Dominik Roblek, Kevin Kilgour, Matt Sharifi, and Mauricio Zuluaga. Fréchet Audio Distance: a reference-free metric for evaluating music enhancement algorithms. In *Proc. Interspeech*, pages 2350–2354, 2019. 6
- [49] Martin Russ. *Sound synthesis and sampling*. Routledge, 2012. 1
- [50] Ville Satopaa, Jeannie Albrecht, David Irwin, and Barath Raghavan. Finding a “kneedle” in a haystack: Detecting knee points in system behavior. In *IEEE Int. Conf. Distr. Comput. Syst. Worksh.*, pages 166–171, 2011. 9
- [51] International Telecommunication Union. Telecommunication Standardization Sector. *Methods for subjective determination of transmission quality*. International Telecommunication Union, 1996. 7, 13
- [52] Ousama A Shaaban, Remzi Yildirim, and Abubaker A Alguttar. Audio deepfake approaches. *IEEE Access*, 11:132652–132682, 2023. 16
- [53] Roy Sheffer and Yossi Adi. I hear your true colors: Image guided audio generation. In *ICASSP*, pages 1–5, 2023. 1, 2, 3, 5, 7, 9
- [54] Zhuoran Shen, Mingyuan Zhang, Haiyu Zhao, Shuai Yi, and Hongsheng Li. Efficient attention: Attention with linear complexities. In *WACV*, pages 3531–3539, 2021. 5, 9
- [55] Shuyang Sun, Runjia Li, Philip Torr, Xiuye Gu, and Siyang Li. CLIP as RNN: segment countless visual concepts without training endeavor. In *CVPR*, pages 13171–13182, 2024. 9
- [56] Haohao Tan. <https://github.com/gudgud96/frechet-audio-distance>, 2024. Website. 6
- [57] Antti Tarvainen and Harri Valpola. Mean teachers are better role models: Weight-averaged consistency targets improve semi-supervised deep learning results. In *NeurIPS*, pages 1195–1204, 2017. 4, 9
- [58] Aaron Van Den Oord, Oriol Vinyals, et al. Neural discrete representation learning. *NeurIPS*, 30, 2017. 2
- [59] Ashish Vaswani, Noam Shazeer, Niki Parmar, Jakob Uszkoreit, Llion Jones, Aidan N. Gomez, Łukasz Kaiser, and Illia Polosukhin. Attention is all you need. In *NeurIPS*, page 6000–6010, 2017. 2
- [60] Heng Wang, Jianbo Ma, Santiago Pascual, Richard Cartwright, and Weidong Cai. V2A-Mapper: a lightweight solution for vision-to-audio generation by connecting foundation models. In *AAAI*, pages 15492–15501, 2024. 1, 2, 3, 5, 7, 9

- [61] Yongqi Wang, Wenxiang Guo, Rongjie Huang, Jiawei Huang, Zehan Wang, Fuming You, Ruiqi Li, and Zhou Zhao. FRIEREN: Efficient video-to-audio generation with rectified flow matching. In *NeurIPS*, 2024. 1, 3
- [62] Mika Westerlund. The emergence of deepfake technology: A review. *Technology innovation management review*, 9(11), 2019. 16
- [63] Ho-Hsiang Wu, Prem Seetharaman, Kundan Kumar, and Juan Pablo Bello. Wav2CLIP: Learning robust audio representations from CLIP. In *ICASSP*, pages 4563–4567, 2022. 6, 15
- [64] Yusong Wu, Ke Chen, Tianyu Zhang, Yuchen Hui, Taylor Berg-Kirkpatrick, and Shlomo Dubnov. Large-scale contrastive language-audio pretraining with feature fusion and keyword-to-caption augmentation. In *ICASSP*, pages 1–5, 2023. 4, 9
- [65] Yazhou Xing, Yingqing He, Zeyue Tian, Xintao Wang, and Qifeng Chen. Seeing and Hearing: open-domain visual-audio generation with diffusion latent aligners. In *CVPR*, pages 7151–7161, 2024. 1, 2, 3, 7, 9
- [66] Qi Yang, Binjie Mao, Zili Wang, Xing Nie, Pengfei Gao, Ying Guo, Cheng Zhen, Pengfei Yan, and Shiming Xiang. Draw an Audio: leveraging multi-instruction for video-to-audio synthesis. *arXiv preprint arXiv:2409.06135*, 2024. 2, 3
- [67] Mingjing Yi and Ming Li. Efficient video to audio mapper with visual scene detection. *arXiv preprint arXiv:2409.09823*, 2024. 2
- [68] Lin Zhang, Shentong Mo, Yijing Zhang, and Pedro Morgado. Audio-synchronized visual animation. In *ECCV*, pages 1–18. Springer, 2024. 7
- [69] Yiming Zhang, Yicheng Gu, Yanhong Zeng, Zhening Xing, Yuancheng Wang, Zhizheng Wu, and Kai Chen. Foley-Crafter: bring silent videos to life with lifelike and synchronized sounds. *arXiv preprint arXiv:2407.01494*, 2024. 1, 3, 7
- [70] Hang Zhao, Chuang Gan, Andrew Rouditchenko, Carl Vondrick, Josh McDermott, and Antonio Torralba. The sound of pixels. In *ECCV*, pages 570–586, 2018. 5, 9
- [71] Yuanjun Zhao, Xianjun Xia, and Roberto Togneri. Applications of deep learning to audio generation. *IEEE Circuits and Systems Magazine*, 19(4):19–38, 2019. 1
- [72] Jinxing Zhou, Jianyuan Wang, Jiayi Zhang, Weixuan Sun, Jing Zhang, Stan Birchfield, Dan Guo, Lingpeng Kong, Meng Wang, and Yiran Zhong. Audio-visual segmentation. In *ECCV*, pages 386–403, 2022. 7
- [73] Yipin Zhou, Zhaowen Wang, Chen Fang, Trung Bui, and Tamara L Berg. Visual to sound: Generating natural sound for videos in the wild. In *CVPR*, pages 3550–3558, 2018. 1, 2